Nano Energy (2014) 3, 152–158

Available online at www.sciencedirect.com

ScienceDirect

journal homepage: www.elsevier.com/locate/nanoenergy

RAPID COMMUNICATION

Elucidating graphene-ionic liquid interfacial region: A combined experimental and computational study

M. Vijayakumar[a,*], Birgit Schwenzer[a], V. Shutthanandan[a], JianZhi Hu[a], Jun Liu[a], Ilhan A. Aksay[b]

[a]Pacific Northwest National Laboratory, Richland, WA-99352, USA
[b]Department of Chemical Engineering, Princeton University, New Jersey- 08544, USA

Received 25 July 2012; received in revised form 25 September 2012; accepted 25 September 2012
Available online 5 October 2012

KEYWORDS
Graphene surface defects;
Ionic liquid;
Interfacial region;
Supercapacitors;
Molecular spectroscopy

Abstract
Graphene and ionic liquids are promising candidates for electrode materials and electrolytes, respectively, for modern energy storage devices such as supercapacitors. Understanding the interactions at the interfacial region between these materials is crucial for optimizing the overall performance and efficiency of supercapacitors. The interfacial region between graphene and an imidazolium-based ionic liquid is analyzed in a combined experimental and computational study. This dual approach reveals that the imidazolium-based cations mostly orient themselves parallel to the graphene surface due to π-π stacking interaction and form a primary interfacial layer, which is subsequently capped by a layer of anions from the ionic liquid. However, it also becomes apparent that the molecular interplay at the interfacial region is highly influenced by functional group defects on the graphene surface, in particular by hydroxyl groups.

Introduction

The interactions between electrode surfaces and an electrolyte are the crucial phenomena behind most modern energy storage devices, such as lithium ion batteries and ultracapacitors. In recent years, graphene (G) has been recognized as a desirable electrode material owing to its large surface area and high electronic conductivity [1,2]. Similarly, room temperature ionic liquids (IL) are outstanding candidates for electrolytes due to their higher electrochemical and thermal stability combined with low toxicity [3]. Consequently, G-IL based composite materials are reported as base materials for a variety of applications including ultracapacitors, solar cells and chemical sensors [4-8]. This spurred considerable interest in understanding the G-IL interfacial region. However, the unique properties of ILs, such as highly

*Corresponding author. Fax: +1 509 371 6546.
E-mail address: vijay@pnnl.gov (M. Vijayakumar).

2211-2855/$ - see front matter © 2012 Elsevier Ltd. All rights reserved.
http://dx.doi.org/10.1016/j.nanoen.2012.09.014

concentrated ionic charges and the asymmetric nature of the ions, combined with lesser-known properties of graphene surfaces result in a complex interfacial region. Recently, some attempts have been made to understand the interaction between G and ILs using computational modelling [9–11]. Despite these efforts, the molecular level structure of G–IL interfacial regions is still unclear due to limitations in computational methods and lack of experimental studies of these materials. Most of the experimental work so far is aimed at demonstrating the respective application, not at studying the interfacial region of the composite material. In addition, theoretical studies reported about G–IL interfacial regions were carried out assuming a perfect defect-free graphene surface, which is far from practical reality. For example, cost effective chemical synthesis methods often lead to the formation of oxygen-containing functional defect groups such as epoxy (C–O–C), carboxyl (O═C–OH) and hydroxyl groups (C–OH) on graphene surfaces [12–14]. Hence it is necessary to study realistic graphene surfaces that include these functional groups, using theoretical and experimental analysis to explore the graphene–ionic liquid interfacial region.

To understand the molecular interaction between the G and IL, a monolayer of 1-butyl-3-methyl-imidazolium ($BMIM^+$) trifluoromethanesulfonate (TfO^-) on graphene surfaces was synthesized (hereafter called as G–IL). This IL monolayer formation enables us to study the molecular level interaction at the interfacial region between graphene and ionic liquid. Subsequently, Nuclear Magnetic Resonance (NMR), X-ray Photoelectron (XPS) and Infrared (FTIR) spectroscopy analyses on this G–IL material were carried out. These analytical results are then correlated with molecular models, which were derived using Density Functional Theory with empirical dispersion correction (DFT-D3) based methods [15]. This combined approach yields a clear view about the G–IL interactions at the interfacial region.

Experimental methods

Materials synthesis

To prepare the G–IL material, 1-butyl-3-methyl-imidazolium ($BMIM^+$) trifluoromethanesulfonate (TfO^-) (99.9% purity; Sigma-Aldrich) and high purity graphene (the oxygen impurity is about 1% *i.e.* C/O ratio of 100; Vorbeck Materials) were used without any further purification. For the synthesis of the G–IL composite material, 2.23 ml of ionic liquid, *i.e.* [$BMIM^+$] (TfO^-), is added into 97.77 ml deionized water and stirred for 4 h at room temperature, then 100 mg of graphene powder (C/O = 100) is added to the solution and stirred for 15 min. The resulting molar ratio of graphene to IL is 1:1.2. The solution is then sonicated for 1 h in 1 s pulse increments using a horn sonicator with a 13 mm tip (Branson Sonifier 450D, 450 W, 55% amplitude). After sonication, the black solution is transferred into test tubes and centrifuged for 10 min at 10,000 rpm. The resulting clear, colorless supernatant is carefully pipetted off, and the black precipitate is dried at 60 °C. Any IL molecule not bound or coordinated to a graphene surface will have been removed with the supernatant because of the very high solubility of the IL in water. Overall, the low molar ratio of *G* to IL (1:1.2) used in this synthesis and the extreme solubility of IL in water ensures the formation of an IL monolayer on the graphene surface. The formation a monolayer coverage of the few-layer graphene surface with IL is analytically confirmed by the absence of sharp peaks in ^1H and ^{19}F NMR (which would represents a liquid component with high rotational freedom, such as residual neat IL; see supplemental information). As control experiments, the same analytical characterization (data not shown) was carried out on as-received graphene and graphene that had been sonicated in pure deionized water for 1 h and then worked up in the same way as the G–IL hybrid material. The absence of any signals attributable to water in the ^1H NMR spectra of the control samples as well as the spectra of the G–IL composite material confirm that the samples were completely dried, and that the presence of water during the synthesis did not affect the surface of the few-layer graphene or the interaction between graphene and the ionic liquid. Furthermore, we can conclude that the water-based synthesis method will not pose a problem when the material will be tested in the water-free environment of a supercapacitor.

Spectroscopic measurements

The ^1H and ^{19}F MAS NMR measurements were performed on a Varian 500 spectrometer (B_0 = 11.7 T and ^1H and ^{19}F Larmor frequency of 500.1 and 470.5 MHz, respectively) with MAS at 12 kHz using 4 mm rotors. The ^1H and ^{19}F chemical shifts are referenced with secondary reference of adamantine (δ = 1.63 ppm) and aqueous solution sodium trifluoroacetate (δ = −76.5 ppm), respectively. The X-ray Photoelectron Spectroscopy (XPS) measurements were performed with a Phi 5000 Versa Probe. This system consists of a monochromatic focused Al Kα X-ray (1486.7 eV) source and a hemispherical analyzer. The aliphatic carbon (*i.e.* C–C bond) C1s peak position is used as reference at 284.5 eV for charge neutralizer correction in XPS spectra. FTIR spectra of pure Ionic liquid, graphene and G–IL hybrid material were recorded with a Nicolet iS10 (Thermo Scientific). The spectra shown were recorded at a resolution of 1 cm^{-1} or higher employing a diamond Smart ITR accessory.

Computational methods

Density functional theory (DFT) based calculations were carried out using the *Amsterdam Density Functional* (ADF-2010) package. The Becke (exchange) + LYP (correlation) based function with recent dispersion correction (DFT-D3) is employed for both geometry and NMR chemical shift calculations [15–18]. All the calculations were carried out using the TZP (triple *Z*, single polarization function, all electron) basis set with the Slater type functional implemented in the ADF program [19]. The organic polyaromatic compound circumcircumcoronene ($C_{96}H_{24}$), which is a polycyclic arene compound with hydrogen termination, is used as starting geometry for the graphene layer [9]. The fully optimized structure of $C_{96}H_{24}$ yields C–C and C–H bond length of 1.42 Å and 1.08 Å, respectively which are in good agreement with literature reported values. For the G–IL molecular structure, a single ion pair of the fully optimized

BMIM TfO molecule is introduced near the center of the graphene model and optimized without any structural constraints. During the optimization process as well as in the final geometry the IL molecule stayed away from the terminal protons, which shows that any effects from the terminal protons are minimal in our $C_{96}H_{24}$ based graphene model. The adsorption energy (ΔE_{obs}) was determined as the difference between the binding energy of the G–IL hybrid material and the sum of the binding energies of the graphene and IL.

Results and discussion

Fig. 1 shows the ^{1}H and ^{19}F NMR spectra of the G–IL material and neat IL measured at room temperature. The ^{1}H spectra of the neat IL shows 8 sharp peaks (numbered 1–8), representing different proton environments within the BMIM cation [20]. In comparison, the ^{1}H MAS spectra of G–IL differs in two aspects, namely significant line broadening and a general peak shift (ca. 1 ppm) towards lower frequency. The observed line broadening under high MAS measurements (see supplemental information) mainly arises from the anisotropic magnetic susceptibility (AMS) effect [21]. In general, the AMS induced line width represents a superposition of different chemical shifts that directly relates to the heterogeneity of the molecular structure in the sample. Hence, the observed line broadening suggests a distribution of BMIM molecular structures at the G–IL interface. Similarly, the ^{1}H peak shifts can be explained based on the effect of the ring current arising from the aromaticity of the graphene layers [22]. According to the aromatic ring chemical shielding (ARCS) theory [23], the isotropic chemical shielding of an atom greatly depends on the radius of the

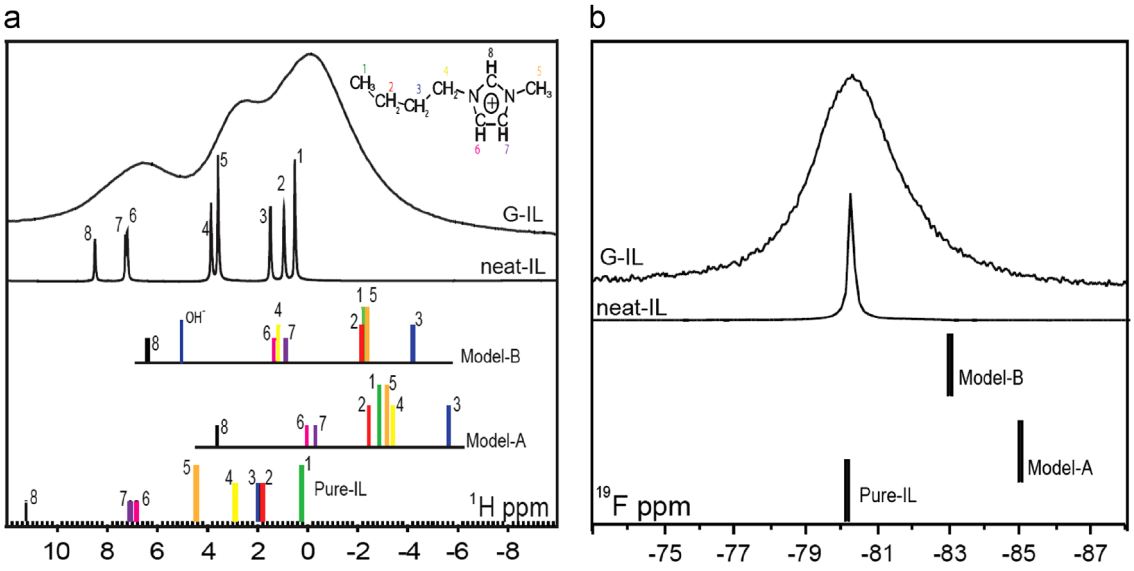

Fig. 1 (a) ^{1}H and (b) ^{19}F MAS NMR spectra of IL and the G–IL material, measured with 12 kHz spinning speed at a magnetic field of 11.7 T. Chemical shifts calculated from DFT-D3 based models are indicated as vertical lines for comparison.

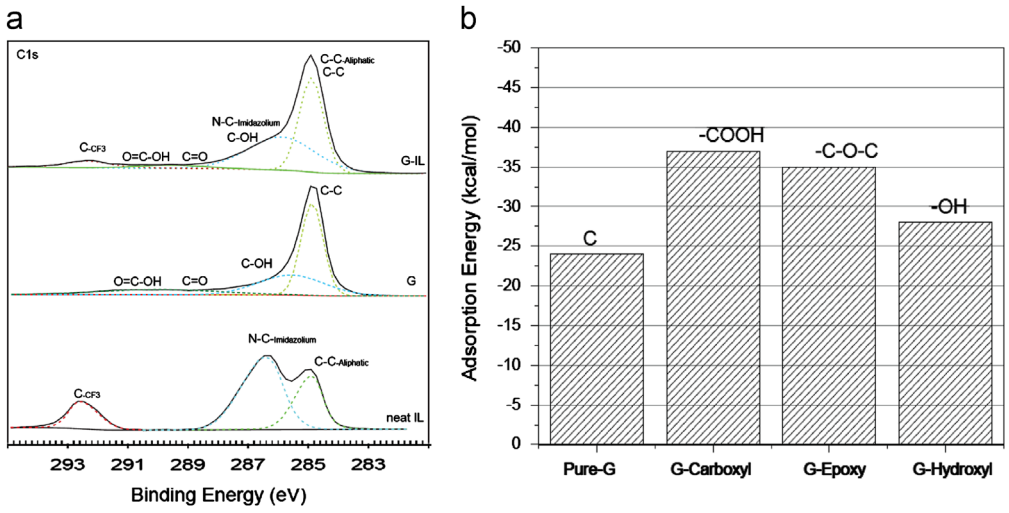

Fig. 2 (a) C1s region in the XPS spectra of the neat IL (bottom), pure graphene (middle) and the G–IL composite material (top). (b) Adsorption energy of an IL molecule absorbed on pure grapheme (left) and graphene with different oxygen-containing functional groups; calculated from BLYP-D3 level DFT theory.

ring current loop and the perpendicular distance of atom from the loop center *i.e.*,

$$\sigma(z) = -\frac{\mu_0}{2}\frac{\partial I_{Ring}}{\partial B_{ext}}\frac{R^2}{\left(z^2+R^2\right)^{3/2}} \quad (1)$$

where R is the radius of the current loop, z is the perpendicular distance from the loop center, $\sigma(z)$ is the z-dependence of the isotropic nuclear magnetic shielding function, and B is the applied magnetic field. This implies that the proton chemical shift will depend on two major factors, namely the distance and the orientation of a proton with respect to the aromatic ring and the strength and radius of the aromatic ring current originate from both graphene and imidazolium. Therefore, ^{1}H peak shift can provide an insight about the distance between BMIM cations and graphene layers (*i.e.* interfacial separation), provided the graphene ring current is known. However the knowledge about the aromatic ring current in layered graphene is limited and known to depend on structural defects in graphene [24]. To overcome this drawback, DFT-D3 theory based models can be employed to understand the molecular structure and orientation of IL molecules on a graphene surface in the presence of functional group defects.

As a first step, any functional groups, possibly present as defects on the graphene surface, are identified by using XPS spectroscopy. Fig. 2(a) shows the XPS spectrum in the C1s region of pure IL, pure graphene (G) and the G–IL composite material. Both, the G and G–IL samples show that three major oxygen-containing functional groups are present on the graphene surface, namely hydroxyl groups (OH), carboxyl groups (COOH) and epoxy groups (C–O–C). This is corroborated by XPS spectra of the O1s region for the respective samples (see supplemental information). Analytical curve fitting of these spectra gave a relative concentration of each defect group: epoxy groups ($<$2%), hydroxyl groups ($\sim$8%) and carboxyl groups ($<$2%). The molecular structure of the G–IL interfacial region with these oxygen containing functional group is computed using ADF 2010 package [25] with the *BLYP-D3* function and all-electron *TZP* basis set. The adsorption energy for an IL molecule on the graphene surface containing each functional group, respectively, is calculated and shown in Fig. 2(b). The comparison of these adsorption energies reveals that graphene with any type of defect group on the surface possesses a relatively lower energy (up to 10 kcal/mol) than pure graphene without any surface defects. This means that the adsorption of IL molecules near an oxygen containing group is more favorable than adsorption on defect-free graphene. These results highlight the importance of the surface functional groups on G–IL interfacial interactions. The next step is to validate these models by comparing with observed NMR chemical shifts. The hydroxyl (OH^-) group is the dominant surface defect group ($\sim$8%) in both pure graphene and G–IL material as evident from C1s and O1s XPS spectra and consequently only hydroxyl group defects will be considered for further analysis. To understand the effect OH^- groups have on G–IL interactions both defect-free and OH^- containing graphene surfaces were considered in the computational study. The computed structures with defect-free graphene (Model-A) or a hydroxyl group containing graphene (Model-B) show that the BMIM cation orients itself parallel to the graphene surface with the butyl chain folded away from the graphene layer (Fig. 3). The distance between the BMIM molecule and the graphene layer is about 3.5 Å (from nitrogen) for both Model-A and B, which is similar to a graphite layer separation of $\sim$3.2 Å. This indicates the adsorption of the BMIM cation is mainly driven by the π–π stacking interaction between the imidazolium ring and graphene. The TfO^- anion, however, is located $\sim$3.5 Å from the defect-free graphene surface (from sulfur) in Model-A, but realigns itself by moving away from the graphene surface, increasing the interfacial separation to $\sim$5.2 Å, in Model-B. This confirms that the presence of hydroxyl group on the graphene surface increases the negative charge of the graphene layer and thereby causes electrostatic repulsion of the TfO^- anion. Now we can validate these models with experimental results and derive the molecular structure at the G–IL interface.

The ^{1}H chemical shifts for the BMIM cation in both models are calculated using the NMR module included in the ADF package. The calculation shows that the ^{1}H peaks shift as much as 6 ppm and 4 ppm towards lower frequency (in comparison with the pure IL spectra) for Model-A and Model-B, respectively (Fig. 1a). It is clear that the current DFT model overestimates the chemical shift values compared with experimental values. This is not surprising considering that the chemical shifts calculated by DFT models has inherent errors associated with the choice of electron basis sets and level of theory used in the calculations. In addition, these calculations are carried out for motionless molecule whereas the experimental NMR spectra are influenced by vibrational and other dynamics of the molecule [26]. Hence more attention should be paid to the trends in the DFT calculated δ values between the compounds rather than to their actual values. Considering this inherent restriction in DFT based chemical shift calculations, our DFT models predict the trend and direction of the chemical shift towards lower frequency fairly well, as evidenced by

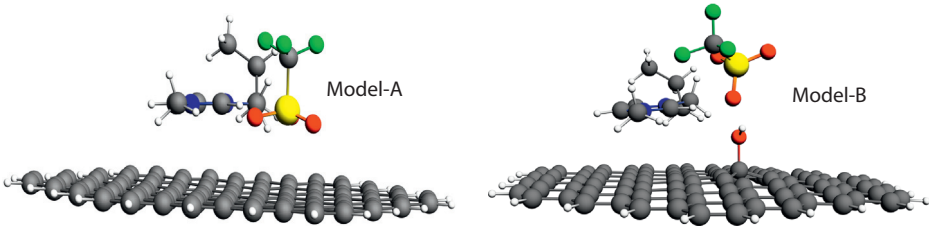

Fig. 3 DFT computed models for an IL molecule close to a pure graphene layer (Model-A) and graphene with a hydroxyl group (Model-B) using BLYP-D3 level theory and TZP (all electron) basis set. The carbon, oxygen, nitrogen, fluorine, sulfate and proton atoms are represented as gray, red, blue, green, yellow and white spheres, respectively.

comparison with the observed shifts in the NMR experiments. In particular, the model for graphene with an OH^- group (Model-B) is closer to the experimental result since it closely represents our G-IL material, where OH^- groups are dominant. This result clearly shows that interaction between graphene and ILs is influenced by functional groups on the graphene surface. Another major result from DFT modeling is that the extent of ^1H peak shift induced by aromatic ring currents greatly depends on the position of the respective atom relative to graphene. This is also in accordance with the ARCS theory discussed earlier. Hence, the experimentally observed NMR peak shift can provide an insight about the IL molecule position with respect to the graphene layer.

Now we can extend this result to analyze the interfacial separation of TfO anion's from graphene. For this, the ^{19}F MAS NMR spectra of the G-IL composite was recorded (Fig. 1b), which shows no significant peak shift (<0.1 ppm) relative to the neat IL. On the other hand, the DFT models A and B predicted a ^{19}F shift of 6 ppm and 3.5 ppm, respectively, towards lower frequency. Again these calculated ^{19}F shifts clearly depend on the degree of interfacial separation between fluorine and grapheme, which is similar to the ^1H NMR data. Hence the absence of a significant ^{19}F shift in the spectra of the G-IL material indicates that the effect of the aromatic ring current from graphene on the TfO^- anion is small. This implies that the TfO^- anion is further away from graphene compared with the BMIM cation. This result agrees with the structure in our Model-B, where the anion moves further away due to the presence of negatively charged hydroxyl groups on the graphene surface. But the interfacial separation of the anion in our G-IL samples might be even higher than the value predicted in Model-B possibly due to the presence of other functional groups such as epoxy and carboxyl groups in our G-IL material.

To further study the G-IL interfacial region, XPS measurements were carried out and the C1s and O1s are the typical region used to identify different chemical environments in Graphene and/or IL compounds. Both C1s and O1s regions shows the presence of hydroxyl, carboxyl and epoxy functional groups in our G-IL material. However the severe overlap of peaks and poor resolution of binding energies restricted a detailed analysis of these regions (see supplemental information). Therefore we focused on the N1s and F1s regions, which can provide information about the BMIM cations and TfO^- anions, respectively. The N1s peak of the G-IL material shows no significant change in binding energy (<0.1 eV), but a reasonable broadening (~ 0.3 eV) compared with the neat IL spectrum (Fig. 4). The broadening of N1s peak of G-IL suggests that the delocalized π electrons in the imidazolium ring are affected due to its interaction with the graphene layers. Such interaction implies significant π-π stacking of the imidazolium ring and graphene. This result validates the parallel alignment of the BMIM cation due to the π- stacking effect discussed in our computational models. In contrast, the F1s peak of G-IL is similar to neat IL spectra both in terms of binding energy and line broadening (Fig. 4b). This indicates that, unlike the BMIM cations, the TfO^- anions of the IL are not affected by the delocalized π electrons from the graphene layers, possibly due to its remoteness from graphene surfaces. These results agree well with our NMR and computational results discussed earlier.

Since we have established, that the anion stays further away from the graphene layer, FTIR analysis focusing on the SO_3 related vibration is best suited to shed light onto the anion's chemical environment. Fig. 4c Model B shows FTIR spectra of the neat IL and the G-IL material in the region from 900-1400 cm^{-1} where vibration peaks originating from the TfO anion are expected (see supplemental information). For example the $\nu_{as}(SO_3)$ asymmetric vibration is observed at 1264 cm^{-1} (vs) and 1276 cm^{-1} (sh), whereas the symmetric vibration $\nu_s(SO_3)$, is observed at 1031 cm^{-1} (vs). It is well known that both asymmetric and symmetric vibrations are sensitive to cation and anion electrostatic interaction in

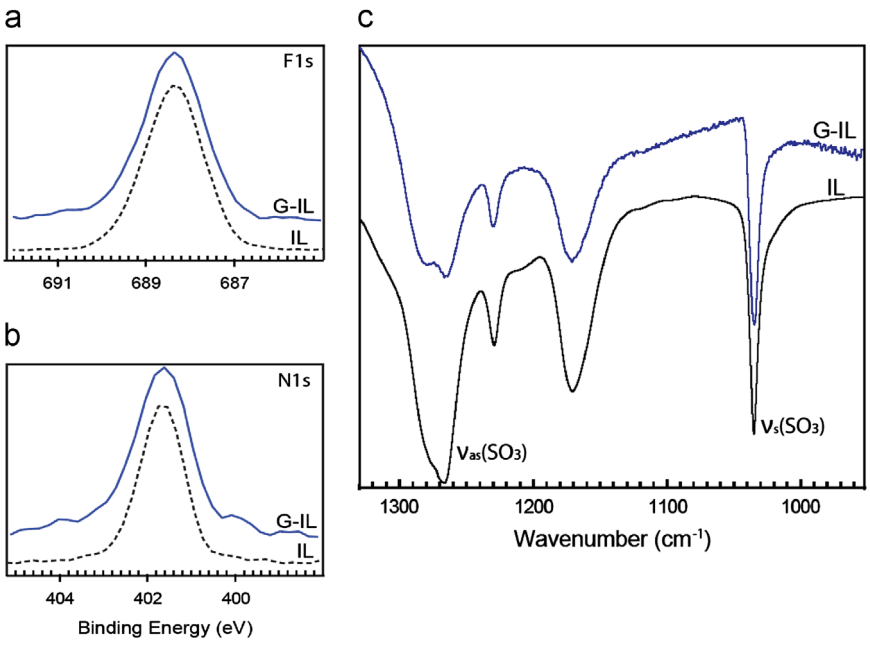

Fig. 4 (a) F1s region, (b) N1s region in XPS spectra of the neat IL (dotted line) and the G-IL material (full line) and (c) FTIR spectra of the neat IL and the G-IL material.

ILs [27]. Interestingly, for the G–IL material the location of both vibrations is very similar to the neat IL, which indicates the BMIM cation and TfO^- anion interaction is prevalent even in G–IL composite materials. Combining these results, we conclude that BMIM cations prefer a closer, parallel orientation to the graphene and form a primary interfacial layer, whereas the anions will stay close to this layer of cations and form a secondary layer, which is in accordance with recent molecular dynamics result [11].

Conclusion

The complex interfacial region between graphene and ionic liquid is analyzed by NMR, XPS and FTIR spectroscopy and the data are correlated with results from dispersion corrected DFT calculations. The insights gained about the effect of oxygen containing functional groups on the G–IL interfacial region can be summarized as follows:

1. The IL molecules, in particular the cations are more likely to get adsorbed near the oxygen containing functional groups (such as hydroxyl) on graphene surface due to relatively lower absorption energy associated with electrostatic attraction.
2. BMIM cations can interact with functional groups on the graphene surface just as they interact with regions of defect-free graphene; on the other hand, TfO^- anions are repelled by negatively charged functional groups on the graphene surface.
3. BMIM cations orient themselves parallel to the graphene layer due to π-π stacking interaction and form a primary interfacial layer, which is subsequently capped by a layer of TfO^- anions.
4. The ionic liquid molecule, i.e. both BMIM cations and TfO^- anions, might exhibit a distribution of molecular orientations near the functional groups on graphene surface.

Our results highlight the influence of hydroxyl groups on G–IL interfacial interactions. For the first time molecular-level experimental observations about the interfacial region in G–IL composites have been correlated with and validated by DFT-based calculations. However, we would like to emphasise that the model used in this study considers only a single hydroxyl group and more detailed studies with clusters of functional groups and multiple IL molecules are needed for an even deeper understanding of the G–IL interfacial region.

Acknowledgments

We thank, Drs. G.L. Graff and S. Thevuthasan for fruitful discussions. We acknowledge Vorbeck Materials for providing the graphene powder for this study. This research work is funded under the open call Laboratory Directed Research and Development Program (LDRD) program at Pacific Northwest National Laboratory (PNNL). PNNL is a multiprogram laboratory operated by Battelle Memorial Institute for the Department of Energy (DOE) under Contract DE-AC05-76RL01830. NMR, XPS and DFT computation work were carried out at Environmental Molecular Sciences Laboratory (www.emsl.pnnl.gov), a national scientific user facility sponsored by the DOE's Office of Biological and Environmental Research.

Appendix A. Supporting information

Supplementary data associated with this article can be found in the online version at http://dx.doi.org/10.1016/j.nanoen.2012.09.014.

References

[1] S. Bai, X. Shen, RSC Advances 2 (2012) 64–98.
[2] S.L. Candelaria, Y. Shao, W. Zhou, X. Li, J. Xiao, J.-G. Zhang, Y. Wang, J. Liu, J. Li, G. Cao, Nano Energy 1 (2012) 195–220.
[3] M. Armand, F. Endres, D.R. MacFarlane, H. Ohno, B. Scrosati, Nature Materials 8 (2009) 621–629.
[4] Y. Chen, X. Zhang, D. Zhang, P. Yu, Y. Ma, Carbon 49 (2011) 573–580.
[5] J. Pu, S. Wan, W. Zhao, Y. Mo, X. Zhang, L. Wang Q. Xue, The Journal of Physical Chemistry C 115 (2011) 13275–13284.
[6] I. Ahmad, U. Khan, Y.K. Gun'ko, Journal of Materials Chemistry 21 (2011) 16990–16996.
[7] H.-J. Choi, S.-M. Jung, J.-M. Seo, D.W. Chang, L. Dai, J.-B. Baek, Nano Energy 1 (2012) 534–551.
[8] Q. Liu, O. Nayfeh, M.H. Nayfeh, S.-T. Yau, Nano Energy 2 (2013) 133–137.
[9] M.H. Ghatee, F. Moosavi, The Journal of Physical Chemistry C 115 (2011) 5626–5636.
[10] Y. Shim, Y. Jung, H.J. Kim, The Journal of Physical Chemistry C 115 (2011) 23574–23583.
[11] M.V. Fedorov, R.M. Lynden-Bell, Physical Chemistry Chemical Physics 14 (2012) 2552–2556.
[12] D. Li, M.B. Muller, S. Gilje, R.B. Kaner, G.G. Wallace, Nature Nanotechnology 3 (2008) 101–105.
[13] J.-A. Yan, M.Y. Chou, Physical Review B 82 (2010) 125403.
[14] L. Lai, L. Wang, H. Yang, N.G. Sahoo, Q.X. Tam, J. Liu, C.K. Poh, S.H. Lim, Z. Shen, J. Lin, Nano Energy.
[15] S. Grimme, J. Antony, S. Ehrlich, H. Krieg, The Journal of Chemical Physics 132 (2010) 154104–154119.
[16] A.D. Becke, Physical Review A 38 (1988) 3098–3100.
[17] C. Lee, W. Yang, R.G. Parr, Physical Review B 37 (1988) 785–789.
[18] S. Grimme, W. Hujo, B. Kirchner, Physical Chemistry Chemical Physics 14 (2012) 4875–4883.
[19] M. Krykunov, T. Ziegler, E.v. Lenthe, International Journal of Quantum Chemistry 109 (2009) 1676–1683.
[20] P. Suarez, A.Z., S. Einloft, J. Dullius, E.L., R. de Souza F., J. Dupont, Journal de Chimie Physique 95 (1998) 1626–1639.
[21] J. Furrer, K. Elbayed, M. Bourdonneau, J. Raya, D. Limal, A. Bianco, M. Piotto, Magnetic Resonance in Chemistry 40 (2002) 123–132.
[22] D.L. Vander Hart, Magnetic susceptibility and high resolution NMR of liquids and solids, Encyclopedia of Magnetic Resonance, John Wiley & Sons, Ltd, 2007.
[23] J. Juselius, D. Sundholm, Physical Chemistry Chemical Physics 1 (1999) 3429–3435.
[24] F. López-Urías, J.A. Rodríguez-Manzo, E. Muñoz-Sandoval, M. Terrones, H. Terrones, Optical Materials 29 (2006) 110–115.
[25] G. te Velde, F.M. Bickelhaupt, E.J. Baerends, C. Fonseca Guerra, S.J.A. van Gisbergen, J.G. Snijders, T. Ziegler, Journal of Computational Chemistry 22 (2001) 931–967.
[26] Z. Atieh, A.R. Allouche, A. Lazariev, D. Van Ormondt, D. Graveron-Demilly, M. Aubert-Frécon, Chemical Physics Letters 492 (2010) 297–301.
[27] W. Huang, R. Frech, R.A. Wheeler, The Journal of Physical Chemistry 98 (1994) 100–110.